Korean J. Chem. Eng., 37(10), 1709-1716 (2020)
DOI: 10.1007/s11814-020-0583-5

pISSN: 0256-1115
eISSN: 1975-7220

Formation of $CaCO_3$ from calcium sources with different anions in single process of CO_2 capture-mineralization

Dea Hyun Moon*, Arti Murnandari*, Omotayo Salawu, Chan-Woo Lee**, Wonhee Lee*, Young Eun Kim*, Ki Tae Park*, Ji Eun Lee*, Jun Eo*, Soon Kwan Jeong*,†, and Min Hye Youn*,†**

*Climate Change Research Division, Korea Institute of Energy Research (KIER), 152 Gajeong-ro, Yuseong-gu, Daejeon 34129, Korea
**Platform Technology Laboratory, Korea Institute of Energy Research (KIER), 152 Gajeong-ro, Yuseong-gu, Daejeon 34129, Korea
(*Received 2 April 2020 • Revised 14 May 2020 • Accepted 15 May 2020*)

Abstract−The single process CO_2 capture-mineralization approach integrates methods of CO_2 absorption using aqueous solvents and mineral carbonation technology to not only remove carbon dioxide quickly, but also to simultaneously produce precipitated calcium carbonate (PCC). To develop a more sustainable process, it is important to extract calcium from inexpensive raw materials such as industrial by-products. The extractant has a significant effect on the quality of the calcium carbonate produced because it determines the anion paired with the calcium cation. In this work, several calcium sources with different anions (Propionate, Acetate, Nitrate and Chloride) were applied in the single process CO_2 capture-mineralization method, and their influence on the polymorph of the obtained $CaCO_3$ was investigated. The $CaCO_3$ produced with inorganic calcium sources predominantly exhibited a calcite structure, while the $CaCO_3$ produced with organic calcium sources had a structure in which vaterite and calcite coexist. This result was in good agreement with our DFT calculations, which indicated the adsorption energy of the organic anions (Propionate and Acetate) were lower than the inorganic anions on the surface of vaterite. Except for chloride with its non-polar nature, in most cases, there was a strong correlation between the polymorph and the adsorption energy calculated for each surface. A mechanism for the polymorph $CaCO_3$ formation in our single process CO_2 capture-mineralization method was proposed after observing crystal formation at low concentration.

Keywords: Calcium Extraction, $CaCO_3$ Polymorphism, CO_2 Carbonation, Calcium Anion, Adsorption Energy, Internal Energy

INTRODUCTION

As international efforts to reduce greenhouse gas emissions accelerate, carbon capture and utilization (CCU) technologies are increasingly recognized as a promising approach because they can convert captured CO_2 into a more useful material instead of simply storing it. However, because carbon dioxide is thermodynamically very stable and has a low energy level, turning it into other substances, such as hydrocarbons, requires the consumption of large amounts of energy [1,2].

Among the various types of CCU technologies, mineralization is very advantageous in terms of energy because it converts CO_2 to carbonates, which have energy levels lower than carbon dioxide. As a result, mineralization is a good way to isolate and store carbon dioxide permanently [3,4]. Mineralization of CO_2 from a metal anion or metal oxide such as calcium, magnesium or iron results in a stable mineral, carbonate, through an exothermic reaction. Indirect carbonation, which includes an extraction process using various solvents, produces a high purity mineral carbonate. Various extractants, including steam [5], hydrochloric acid [6], ammonium chloride [7], sulfuric acid [8], acetic acid [9], and mixtures of solvent [10] have been studied, and the metal salt that can be obtained is determined by the type of extractant used.

Recently, many studies have been conducted to permanently sequester carbon dioxide using various calcium sources, such as industrial by-products [7,11-13]. In particular, sustainable and reliable CCUS technologies have been proposed [14-17], which attempt to quickly capture CO_2 gases and convert them into useful materials. The combination of CCS technology and mineralization has many advantages from the viewpoint of feedstock flexibility, capital requirements and operating costs, high value product, and an alternative to direct storage.

In our previous work, we proposed a single process for CO_2 capture and mineralization which produced a precipitated calcium carbonate (PCC) [15-18]. We also developed a process that was repeatable via chemical regeneration [19]. In that system, an amine solvent was used to absorb CO_2 and then this CO_2 saturated amine was reacted simultaneously with calcium sources for mineralization. The use of amine in the mineralization amplified the carbonation activity. The use of a calcium source also led to facile CO_2 desorption from the amine during regeneration. Moreover, $CaCO_3$ was produced as a value-added product. This process is also supe-

†To whom correspondence should be addressed.
E-mail: mhyoun@kier.re.kr, jeongsk@kier.re.kr
‡Min Hye Youn and Soon Kwan Jeong contributed equally to this work and share corresponding authorship.

rior to conventional amine scrubbing processes because it can be performed at low temperature, thus reducing the amount of energy required to regenerate the CO_2. Also, PCC production can be accomplished at low pressure, such as ambient conditions.

One of the more important factors in the continuous capture-mineralization process, however, is the type of anion used with the calcium cation. It can determine the type of extraction solvent and affect the overall reaction system, remaining after the precipitation of the calcium carbonate. Many researchers have studied indirect carbonation for calcium extraction from solid wastes with high calcium content [6,20]. In most cases, organic, inorganic acid and mixtures have been used for the efficient extraction of calcium ions. However, in mineral carbonation the extracted cations are used with paired anions. For further process development it is necessary to check how the anion, in combination with calcium, affects the mineral carbonation.

This work investigated how various calcium sources with different anions affected $CaCO_3$ formation, and how they transformed polymorphism via the single process CO_2 capture-mineralization method. The thermodynamic aspects were investigated by simulating molecular interactions and analyzing methods of controlling the $CaCO_3$ morphology changes. The results were then discussed in relation to further development of the process.

EXPERIMENTAL SECTION

1. Single Process of CO_2 Capture-mineralization Procedure

An AMP (2-amino-2-methyl-1-propanol, 90%, Aldrich) solution was used as the absorbent to absorb CO_2 gas in a 500 mL glass semi-batch reactor. 250 mL of 10 wt% AMP aqueous solution was prepared. A mixture gas of 30% CO_2 and 70% N_2 was introduced into the AMP solution at 40 °C and mixed using a magnetic stirrer operating at 450 rpm. When the concentration of the outlet CO_2 gas reached a steady state, the prepared calcium source was injected into the reactor with a syringe. The electrical conductivity was measured using an ISE probe in the reactor. After injecting the calcium source, precipitation and crystallization reactions were allowed to proceed for 90 min and 24 hr, respectively. Then, to immediately stop the reaction on the powder, the obtained samples were washed with acetone while vacuum filtering, and dried in an oven at 60 °C for 24 hr.

2. Materials & Characterization

The calcium sources used were calcium propionate (97% purity, Sigma Aldrich), calcium acetate (99%, Sigma Aldrich), calcium chloride anhydrous granular (93% purity, Sigma Aldrich), and calcium nitrate tetrahydrate (99% purity, Sigma Aldrich).

$CaCO_3$ powder obtained from the process was analyzed with a scanning electron micrograph (FE SEM, Hitachi/S-4700), X-Ray diffraction (XRD, Rigaku/DMax-2500), and by Brunauer-Emmett-Teller method (BET, Micromeritics/ASAP-2020).

3. Simulation of Molecular Interactions

To shed more light on the experimental results for vaterite and calcite, we applied a first principles method with the Vienna *ab initio* simulation package (VASP) [21,22] to study the adsorption energetics in these compounds. The electronic exchange-correlations were simulated within the generalized gradient approximation (GGA) as described by Perdew, Burke and Ernzehof (PBE) [23]. Relaxation of the systems was carried out using the conjugate-gradient method until the total energy was less than 10^{-3} eV/system. A 3×3×1 Monkhorst-Pack grid of K points and an energy cut-off of 400 eV were employed for geometric optimization.

For the slab calculations, we cleaved the (010) and $(10\bar{1}4)$ surfaces for vaterite and calcite, respectively. Previous experimental and theoretical studies reported that these two surfaces are the most stable compounds [24,25]. The number of layers to consider for our adsorption of molecules was optimized by calculating surface energies for different numbers of layers. We found the surface energy of seven layers (vaterite) and five layers (calcite) converged, while a higher number of layers produced a surface energy difference of just 0.04 J/m^2. The most stable configuration for the adsorption of molecules was obtained by considering a number of molecular geometries, which were allowed to interact with the surface in such a way that the functional groups interacted directly with the surface atoms. They were modelled using a (2×2) supercell and a 23 Å vacuum, with the bottom two layers fixed in the bulk positions, while the layers above were allowed to relax. The adsorption energy was calculated to be

$$E_{ads}\ (eV)=E_{mol/surf}-E_{mol}-E_{surf} \quad (1)$$

where $E_{mol/surf}$, E_{mol} and E_{surf} represent the energies of the surface with a molecule, an isolated molecule, and the slab, respectively. A negative E_{ads} indicates an exothermic process, and a more negative value implies a stronger interaction with the surface, while a positive adsorption energy represents an unstable process. The effect of dispersion is well described by the DFT-D approach [26] and its impact was investigated in the present study. Adsorption energy calculations took this into account by substituting the energies in Eq. (1) with values from the calculations with a van der Waals correction.

RESULTS AND DISCUSSION

1. Polymorphism of $CaCO_3$ Produced from Various Calcium Sources (Ca_X, X=Propionate, Acetate, Nitrate and Chloride) in the Single Process CO_2 Capture-Mineralization Method

Based on our previous results [16,17], the single process CO_2 capture-mineralization method was conducted in a semi-batch reactor. After sufficiently saturating the CO_2 gas in the aqueous AMP solution, the calcium source (Ca_X) was injected with a CO_2 loading to amine mole ratio of 1 : 1. Since all of the tested calcium sources were water soluble, they were easily ionized by water. The ionized calcium (Ca^{2+}) then rapidly combined with bicarbonate (HCO_3^-) to form the precipitated calcium carbonate. In the AMP solution, because of the alkyl group in its structure, unstable carbamate is formed and hydrolyzes easily to bicarbonate. This favors the formation of calcium carbonate [27]. The CO_2 capture-mineralization reaction in the AMP system can be summarized as follows.

$$2C_4H_{11}NO_{(aq)}+CO_{2(g)} \rightleftharpoons C_4H_9NHCOO^-_{(aq)}+C_4H_9NH_3^+{}_{(aq)} \quad (2)$$

$$C_4H_9NHCOO^-_{(aq)}+H_2O_{(l)} \rightleftharpoons HCO_3^-{}_{(aq)}+C_4H_9NH_{2(aq)} \quad (3)$$

$$Ca(X)_{2(aq)} \rightleftharpoons Ca^{2+}{}_{(aq)}+2(X)^-_{(aq)};\ (X=Cl,\ NO_3,\ CH_3COO,\ C_3H_5OO) \quad (4)$$

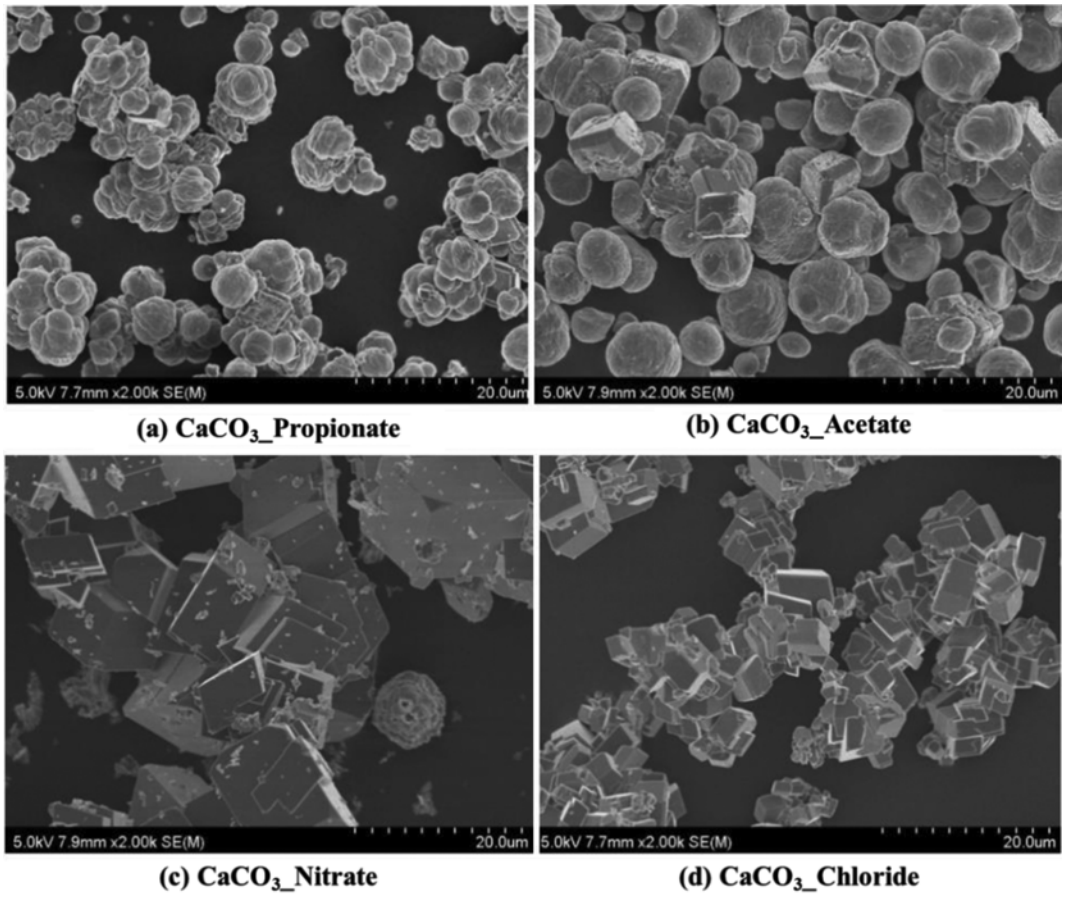

Fig. 1. SEM images of $CaCO_3$_X, X=(a) propionate, (b) acetate, (c) nitrate, and (d) chloride.

$$Ca^{2+}_{(aq)}+2HCO_3^-{}_{(aq)} \rightleftharpoons Ca(HCO_3)_{2(aq)} \quad (5)$$

$$Ca(HCO_3)_{2(aq)} \rightleftharpoons CaCO_{3(s)}+CO_{2(aq)}+H_2O_{(l)} \quad (6)$$

$$CO_{2(aq)} \rightleftharpoons CO_{2(g)} \quad (7)$$

As indicated in Eq. (4), the calcium ion is present with a paired anion (X) in the aqueous solution so that its properties affect the formation of calcium carbonate. As shown in Fig. S1, the calcium source (Ca_X) used in this study has a different structure and molecular formula. In addition, Ca_Acetate and Ca_Propionate are organic calcium groups, while Ca_Chloride, Ca_Nitrate are inorganic calcium groups; inorganic calcium has a particularly less bulky structure and tends to form a strong acid when dissolved in water [28]. Fig. 1 shows SEM images of the calcium carbonates ($CaCO_3$_X) obtained using the CO_2 capture-mineralization reaction following a change in calcium anion (X). For the organic anions propionate and acetate, a globular calcium carbonate was dominant, whereas in the case of inorganic anions nitrate and chloride, a mainly cubic calcium carbonate was produced. This result is similar to the obtained XRD pattern shown in Fig. 2, where the calcium carbonate produced by inorganic anions exhibits a complete calcite structure, while the calcium carbonate produced by organic anions has a structure in which vaterite and calcite coexist.

In addition, the surface area of the produced $CaCO_3$ decreased in the following order: Ca_Propionate (17.1 m^2/g)>Ca_Acetate (16.2 m^2/g)>Ca_Nitrate (0.8 m^2/g)>Ca_Chloride (0.4 m^2/g). These results can be explained by the change in the conductivity of the solution, as shown in Fig. 3. When the CO_2 gas was introduced into the reactor within the AMP solution, conductivity gradually increased. After saturating CO_2 sufficiently, until the conductivity of the AMP solution did not change any more, the prepared calcium sources

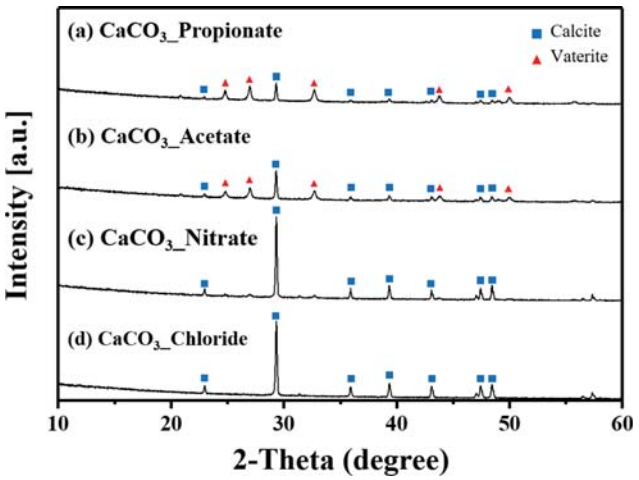

Fig. 2. XRD patterns of $CaCO_3$_X, X=(a) propionate, (b) acetate, (c) nitrate, and (d) chloride.

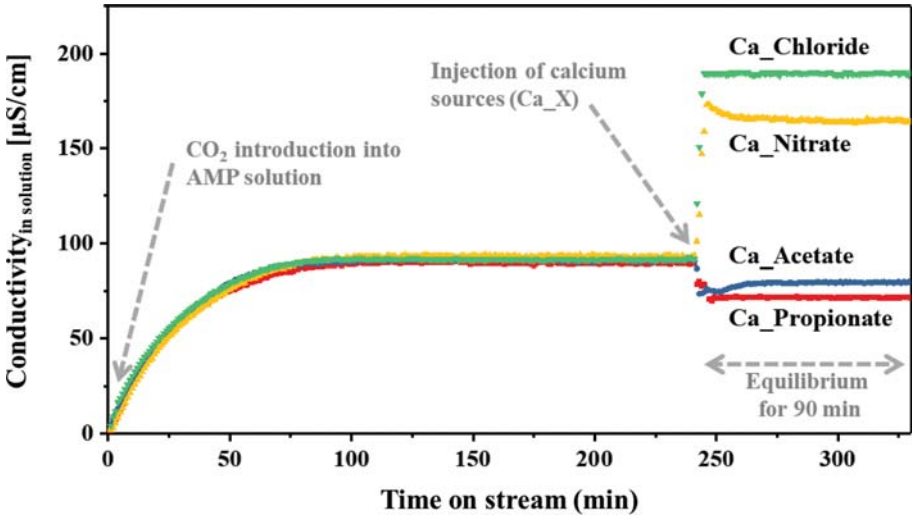

Fig. 3. Comparison of conductivity for different calcium sources (Ca_X, X=propionate, acetate, nitrate and chloride) during the single process CO_2 capture-mineralization in an AMP system.

(Ca_X) were injected. It was observed that the conductivity of the solution varied depending on the type of calcium sources. For the organic calcium groups, Ca_Acetate and Ca_Propionate, a slight decrease in conductivity was measured across the solution. On the other hand, for the inorganic calcium groups, Ca_Chloride and Ca_Nitrate, there was a rapid change to high conductivity. This change in conductivity is caused by the calcium and the disassociated anion (X) in the aqueous solution. An anion with different activity coefficients may alter the total energy of the AMP system, which may affect the formation of calcium carbonate.

From the XRD and SEM results, the structure of the calcium source and variation in conductivity, it can be inferred that an organic bulky structure and lower conductivity is more advantageous for the production of spherical vaterite $CaCO_3$ with a greater surface area. In contrast, inorganic calcium sources (Ca_Nitrate and Ca_Chloride) which form nitrate and chlorine ions, respectively, induce the production of cubic calcite $CaCO_3$.

2. Adsorption Energy Calculation for Various Calcium Sources (Ca_X, X=Propionate, Acetate, Nitrate and Chloride) on the Surface of $CaCO_3$

Using the experimental results, the effects of the molecular interactions in the system were more deeply investigated by simulation. To validate our procedure, we compared our calculated bulk structural parameters with those from experiments and previous calculations (see Table 1). Our obtained lattice parameters agreed well with both [29,30]. From our calculation of the surface energy needed to obtain the optimum number of layers for molecular adsorption, we found that the surface energy of calcite (0.41 J/m^2) was always lower than that of vaterite (0.53 J/m^2). This is in qualitative agreement with previous DFT and molecular dynamics simulations [31,32].

Table 1. Calculated and experimental lattice parameters for vaterite and calcite bulk structures

Lattice constant (Å)	a (Expt.)	b (Expt.)	c (Expt.)
Vaterite	6.97 (7.12)	6.97 (7.12)	25.16 (25.54)
Calcite	4.96 (4.99)	4.96 (4.99)	16.95 (17.06)

The calculated adsorption energies with and without a van der Waals correction are presented in Fig. 4. The calculated values ranged from −0.92 to 2.40 eV for vaterite and −0.81 to 0.08 eV for calcite. These values were compared with previously obtained values for small molecules [33,34]. The magnitude of the adsorption energy partially depends on the electrostatic interaction between the O atom of the molecule and the Ca atom at the surface. The effect of the dispersion interaction between the molecule and the surface is also key to determining the magnitude of the adsorption energy [35].

For all cases considered, the adsorption energy was lower with the DFT-D2 method, which highlights the contribution of dispersion in the adsorption process. This is a peculiar scenario for $CaCO_3$ polymorphs. Okhrimenko et al. reported that adsorption energy values included a very large dispersion contribution, which was

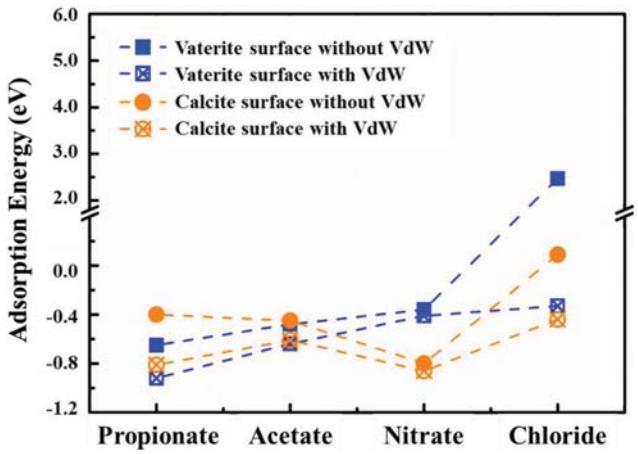

Fig. 4. The adsorption energy for different molecules on vaterite and calcite surfaces with and without van der Waals correction included.

about 30% of the adsorption energy for the case of propanol on calcite [35]. Our investigation revealed that larger molecules are more easily adsorbed on a vaterite surface irrespective of the dispersion effect. Generally, organic molecules have lower adsorption energies on a vaterite surface. To be specific, propionate had the lowest adsorption energy among the tested anions (X) on the vaterite surface, followed by another organic molecule, acetate. On the other hand, chloride was found to have the highest adsorption energy, much higher than nitrate.

In fact, the calculated adsorption energy suggests the instability of the process. For chloride, this unusually high value might be related to the non-polar nature of the chloride molecule, and this was particularly true for our case, since the inclusion of the van der Waals interaction greatly reduced the adsorption energy [35]. Even though the dispersion effect was observed in all other cases, we found the chloride case to be most affected. To further strengthen our inference that the bonding nature of chloride is a potential cause, we found a similarly high adsorption energy for chloride on calcite.

For calcite, chloride adsorption was also found to be the most difficult case, although the adsorption energy was significantly lower than that calculated for vaterite. Also, while the inclusion of the van der Waals correction reduced the adsorption energy, adsorption was still found to be higher than those of other molecules. The fact that the dispersion interaction was very high for chloride shows that without this correction term added, the obtained structure is highly unstable. Taking the dispersion into account implies that the adsorption energy for chloride on the vaterite surface compares reasonably well with that obtained for calcite.

Unlike the case for vaterite, where organic molecules have the lowest adsorption energy values, we found nitrate was most easily adsorbed on calcite. The morphology of the surface of the calcite is different from that of the vaterite and this could be a reason for the marked difference in the adsorption energetics of the two compounds. The order of adsorption energy for calcite was: Propionate >Acetate>Nitrate (see Fig. 4). It is worth noting that the dispersion effect, although very pronounced in the case of chloride adsorption, was found in all of the molecules considered, but was very weak for nitrate.

Indeed, the morphology of the surface plays a significant role in the adsorption energetics of compounds, and we found this to be the case for vaterite and calcite. Vaterite had its lowest surface energy in a model terminated by CO_3 while the calcite surface was characterized by uncoordinated bonding of Ca and CO_3 atoms. Our analysis and findings with respect to the adsorption of these compounds were consistent with our experimental observations. We found a strong correlation between the adsorption energy and the morphology of $CaCO_3$. With the exception of chloride (on calcite), the order of adsorption energy strongly fit our experimental findings. Furthermore, the easier adsorption of chloride and nitrate on calcite correlates to the formation of calcite over vaterite. Also, propionate and acetate's lower adsorption energy for vaterite correlates with the formation of vaterite over calcite when these sources are used.

3. Effect of Calcium Sources (Ca_X, X=Propionate, Acetate, Nitrate and Chloride) on the Polymorphism of $CaCO_3$

To investigate the formation and transport of $CaCO_3$ in more detail, we observed crystal generation using FE-SEM and XRD under very low concentration conditions (Ca/CO_2=0.1) with and without ageing procedure. Unlike the supersaturated condition, reaction can be kinetically controlled at low concentrations. The organic calcium sources Ca_Propionate and Ca_Acetate have a relatively high surface area and rough surface due to the high surface energy, resulting from the bulky structure of the organic molecules. These high surface energy levels induced pine-cone like or spherulitic polycrystalline systems, and ultimately the vaterite phase was formed. At the same time (after CO_2 equilibrium for 90 min) in low concentration (Fig. 5), calcite was formed through polycrystalline vaterite, while in high concentration (Fig. 1) mono-crystalline calcite was formed directly in the system. Calcite is formed when the energy available is high enough to produce a supercritical nucleus, while with lower availability energy, vaterite is formed, which also causes the vaterite phase to be in a stable state [35-37].

The driving force for the formation of the calcium carbonate polymorph is Gibbs free energy, while going from a supersaturated condition to equilibrium [35]. Gibbs energy in constant temperature and pressure is determined by the change in internal energy less the change in entropy at a certain temperature. Stabilization of

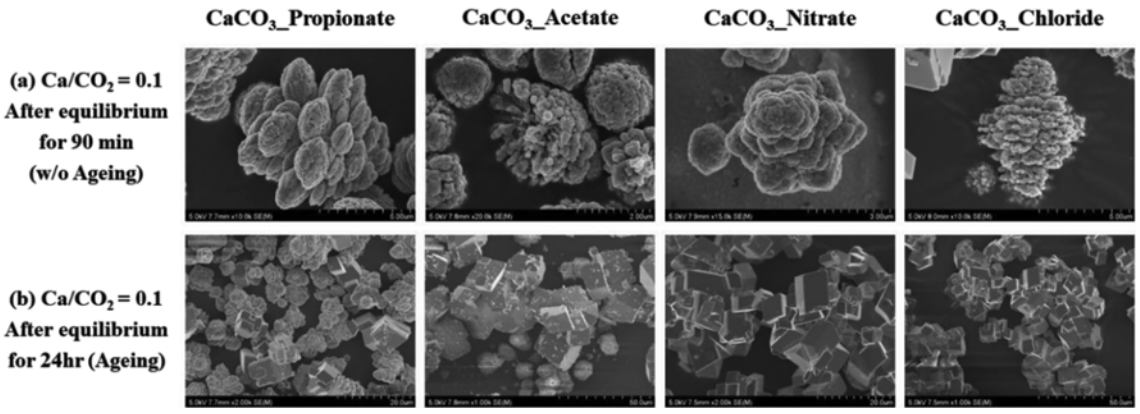

Fig. 5. SEM Images of $CaCO_3$_X with different ageing procedures: (a) After equilibrium for 90 min (without ageing) and (b) after equilibrium for 24 hr (with ageing).

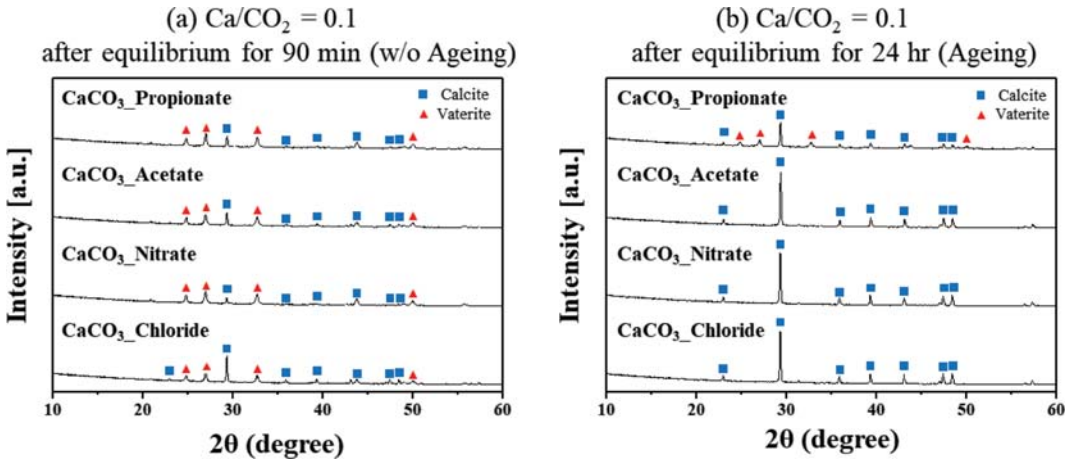

Fig. 6. XRD Patterns of $CaCO_3$_X with different ageing procedures: (a) After equilibrium for 90 min (without ageing) and (b) after equilibrium for 24 hr (with ageing).

the Gibbs energy can be observed in a system by monitoring the solid product phase without ageing (the reaction was stopped after CO_2 equilibrium for 90 min as in Fig. 3) and with ageing (the reaction was stopped 24 hr after CO_2 equilibrium). This can stop the process of crystal growth by immediately ending/terminating the sedimentation reaction through acetone drying.

Figs. 5 and 6 show the SEM images and XRD patterns of calcium carbonate obtained after (a) 90 min (without aging) and (b) 24 hr (with aging) after reaching CO_2 equilibrium at low Ca/CO_2 concentration (Ca/CO_2=0.1), respectively. At low calcium concentrations, most of the observed calcium carbonate is vaterite phase. When precipitation time is short (without aging), vaterite is formed by rapid precipitation, and controlled by kinetic reaction. But, vaterite with a metastable phase can be transformed to calcite by the free energy available in the chemical reaction.

After CO_2 equilibrium for 24 hr (with aging), however, the calcite phase was predominantly observed in the system because the precipitation reaction wants to reach a thermodynamically stable state. These results were in good agreement with the DFT calculations and interpretation mentioned earlier in Fig. 4. The observation that calcite was not fully recovered in calcium propionate after ageing, as discussed above, can be linked to the lower adsorption energy on the vaterite surface compared to the calcite surface.

The tendency of calcite formation can be explained by the internal energy needed for the single process CO_2 capture-mineralization system. The internal energies of the formation for calcite and vaterite were calculated based solely on the molecular structure in the reaction as listed in Table 2. All of the internal energy calculations showed that calcite needed lower energy than vaterite; thus, calcite was always found in all the calcium source systems. As a consequence, calcite in a thermodynamically stable state was constantly produced in the AMP-Ca system.

Table 2. Internal energy of the formation for calcite and vaterite in the single process CO_2 capture-mineralization

Internal energy of formation (eV)				
Ca^{2+} source	Ca_Propionate	Ca_Acetate	Ca_Nitrate	Ca_Chloride
Vaterite	3.765	2.941	3.334	3.635
Calcite	3.625	2.802	3.19	3.495

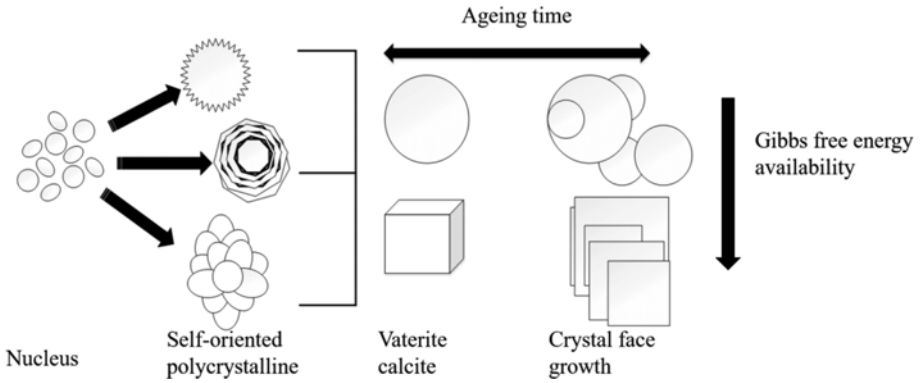

Fig. 7. Mechanism of $CaCO_3$ polymorphism under various calcium sources in the single process of CO_2 capture-mineralization.

4. Proposed Mechanism of $CaCO_3$ Polymorphism in the Single Process CO_2 Capture-mineralization

The formation of calcium carbonate in the single process CO_2 capture-mineralization begins with a nucleus burst in a supersaturated solution, continues by precursor formation, and a self-aggregated polycrystalline, mesocrystal, then stable crystal structure is formed. In a single process and mineralization system using various calcium sources (X), polymorphism is found with a mixture of calcite and vaterite as the product. Crystallized calcite is usually mono-crystalline with well-faceted particles, while vaterite can be produced through nano-aggregation or crystal growth [28,38].

In the early stages of crystallization, vaterite was found to form in all of the systems by spherulitic growth instead of nano-aggregation. The nuclei formed in the system under supersaturated conditions and assembled themselves in a certain polycrystalline form. A polycrystallite formed under high surface energy is not stable, and thus it tried to form a single crystal, such as vaterite and calcite, which is more favorable. Through this mechanism, the calcium carbonate crystal formed in the system tried to reach equilibrium with the lowest free energy available. Then, to reduce the overall energy availability, the crystal surfaces attached together and grew. This mechanism is illustrated in Fig. 7.

CONCLUSIONS

The polymorph $CaCO_3$ formation in the AMP absorption system using various calcium sources (Ca_X, X=Propionate, Acetate, Nitrate and Chloride) combined with anion (X) was investigated. In presence of AMP solution, carbon dioxide is rapidly converted to bicarbonate, which reacts with ionized calcium ion to produce the precipitated $CaCO_3$. These dissociated anions (X) affect the morphology of calcium carbonate produced. In the case of Propionate and Acetate, organic anions, a globular calcium carbonate was dominant, whereas Nitrate and Chloride, inorganic anions, mainly cubic form of calcium carbonate was produced. After observing the mechanism of $CaCO_3$ polymorphism under low concentration conditions with a time difference, the nucleus produced under supersaturated conditions initially formed a self-assembled polycrystalline, which resulted in a difference in polymerization. Most calcium sources initially produce meta-stable vateraite $CaCO_3$, but as they reach equilibrium they have a tendency to switch to calcite, a thermodynamically stable low energy state. This matched the results of absorption energy calculation using DFT and confirmed that low absorption energy is closely related to the production of vaterite.

ACKNOWLEDGEMENT

This work was supported by the Energy Demand Side Management Program of the Korea Institute of Energy Technology Evaluation and Planning (KETEP) granted financial resource from the Ministry of Trade, Industry & Energy, Republic of Korea (No. 20182010202100).

SUPPORTING INFORMATION

Additional information as noted in the text. This information is available via the Internet at http://www.springer.com/chemistry/journal/11814.

REFERENCES

1. S. M. Jarvis and S. Samsatli, *Renew. Sustain. Energy Rev.*, **85**, 46 (2018).
2. R. M. Cuéllar-Franca and A. Azapagic, *J. CO2 Util.*, **9**, 82 (2015).
3. A. Sanna, M. Uibu, G. Caramanna, R. Kuusik and M. M. Maroto-Valer, *Chem. Soc. Rev.*, **43**, 8049 (2014).
4. G. A. Bhaduri and L. Šiller, *Catal. Sci. Technol.*, **3**, 1234 (2013).
5. R. Zevenhoven, S. Teir and S. Eloneva, *Proc. 19th Int. Conf. Efficiency Costs, Optimization, Simulation and Environmental Impact of Energy Systems*, **33**, 1661 (2006).
6. S. M. Lee, S. H. Lee, S. K. Jeong, M. H. Youn, D. D. Nguyen, S. W. Chang and S. S. Kim, *J. Ind. Eng. Chem.*, **53**, 233 (2017).
7. Y. Sun, M. S. Yao, J. P. Zhang and G. Yang, *Chem. Eng. J.*, **173**, 437 (2011).
8. Q. Zhao, C. J. Liu, M. F. Jiang, H. Saxén and R. Zevenhoven, *Miner. Eng.*, **79**, 116 (2015).
9. S. Teir, H. Revitzer, S. Eloneva, C. J. Fogelholm and R. Zevenhoven, *Int. J. Miner. Process.*, **83**, 36 (2007).
10. A. H. A. Park and L. S. Fan, *Chem. Eng. Sci.*, **59**, 5241 (2004).
11. M. Ibrahim, M. El-Naas, A. Benamor, S. Al-Sobhi and Z. Zhang, *Processes*, **7**, 115 (2019).
12. A. Alamdari, A. Alamdari and D. Mowla, *J. Ind. Eng. Chem.*, **20**, 3480 (2014).
13. A. Iizuka, M. Fujii, A. Yamasaki and Y. Yanagisawa, *Ind. Eng. Chem. Res.*, **43**, 7880 (2004).
14. A. M. López-Periago, R. Pacciani, C. García-González, L. F. Vega and C. Domingo, *J. Supercrit. Fluids*, **52**, 298 (2010).
15. M. Vinoba, M. Bhagiyalakshmi, S. Y. Choi, K. T. Park, H. J. Kim and S. K. Jeong, *J. Phys. Chem. C*, **118**, 17556 (2014).
16. M. Arti, M. H. Youn, K. T. Park, H. J. Kim, Y. E. Kim and S. K. Jeong, *Energy Fuels*, **31**, 763 (2017).
17. A. Murnandari, J. M. Kang, M. H. Youn, K. T. Park, H. J. Kim, S. P. Kang and S. K. Jeong, *Korean J. Chem. Eng.*, **34**, 935 (2017).
18. M. Vinoba, M. Bhagiyalakshmi, A. N. Grace, D. H. Chu, S. C. Nam, Y. Yoon, S. H. Yoon and S. K. Jeong, *Langmuir*, **29**, 15655 (2013).
19. J. M. Kang, A. Murnandari, M. H. Youn, W. Lee, K. T. Park, Y. E. Kim, H. J. Kim, S. P. Kang, J. H. Lee and S. K. Jeong, *Chem. Eng. J.*, **335**, 338 (2018).
20. W. Bao, H. Li and Z. Yi, *Ind. Eng. Chem. Res.*, **49**, 2055 (2010).
21. G. Kresse and D. Joubert, *Phys. Rev. B*, **59**, 1758 (1999).
22. G. Kresse and J. Furthmüller, *Phys. Rev. B*, **54**, 11169 (1996).
23. J. P. Perdew, K. Burke and M. Ernzerhof, *Phys. Rev. Lett.*, **78**, 1396 (1997).
24. Y. Liang, A. S. Lea, D. R. Baer and M. H. Engelhard, *Surf. Sci.*, **351**, 172 (1996).
25. A. M. Bano, P. M. Rodger and D. Quigley, *Langmuir*, **30**, 7513 (2014).
26. S. Grimme, J. Antony, S. Ehrlich and H. Krieg, *J. Chem. Phys.*, **132**, 154104 (2010).
27. H. M. Stowe, L. Vilčiauskas, E. Paek and G. S. Hwang, *Phys. Chem. Chem. Phys.*, **17**, 29184 (2015).
28. J. P. Andreassen, *J. Cryst. Growth*, **274**, 256 (2005).
29. J. Balmain, B. Hannoyer and E. Lopez, *J. Biomed. Mater. Res.*, **48**,

342 (1999).
30. E. N. Maslen, V. A. Streltsov and N. R. Streltsova, *Acta Crystallogr. Sect. B*, **49**, 636 (1993).
31. D. M. Duffy and J. H. Harding, *J. Mater. Chem.*, **12**, 3419 (2002).
32. N. H. de Leeuw and S. C. Parker, *J. Phys. Chem. B*, **102**, 2914 (1998).
33. J. S. Lardge, D. M. Duffy and M. J. Gillan, *J. Phys. Chem. C*, **113**, 7207 (2009).
34. E. Ataman, M. P. Andersson, M. Ceccato, N. Bovet and S. L. S. Stipp, *J. Phys. Chem. C*, **120**, 16586 (2016).
35. D. V. Okhrimenko, J. Nissenbaum, M. P. Andersson, M. H. M. Olsson and S. L. S. Stipp, *Langmuir*, **29**, 11062 (2013).
36. D. Kralj, L. Brečević and A. E. Nielsen, *J. Cryst. Growth*, **104**, 793 (1990).
37. D. Kralj, L. Brecević and A. E. Nielsen, *J. Cryst. Growth*, **143**, 269 (1994).
38. D. B. Trushina, T. V. Bukreeva, M. V. Kovalchuk and M. N. Antipina, *Mater. Sci. Eng. C*, **45**, 644 (2015).